Good Practice Guide for the Analysis of High Energy Trapped Particles Measurements and Simulation of their Interaction with the Atmosphere

Alexandre Winant, Viviane Pierrard, Edith Botek

February 29, 2024

Abstract

This Good Practice Guide intends to and summarize the best way to estimate the particle fluxes using satellite measurements and the simulations of their interactions with the atmosphere. This guide written in the framework of the project EURAMET Biosphere is made available on the project's website and promoted at the project's workshops/training events so that users in the space physics, radiation and atmospheric communities can easily access these documents for reference and to implement the methods for estimations of spatial energetic fluxes of particles and for atmospheric investigations developed in the project.

Contents

List of Figures

List of Acronyms

Chapter 1

Introduction

This manuscript is a first attempt to develop a good practice guide for the analysis of measurements from space born spectrometers and particle telescopes that measure differential and/or integral flux of high energy particles trapped in the radiation belts. The main objective of this guide is to help inexperienced researchers in the field to get a used to treating with space borne data products which in some case are difficult to use if they are not handled with precaution. As a results, some error in the data analysis or in their interpretation may arise. Thus, this manuscript is mainly addressed to newcomers in the field of the space physics, and more particularly to the Radiation Belts (RBs).

This first section aims to provide to the reader a basic understanding of the complex environment of the Earth, from the Interplanetary Magnetic Field (IMF) to the motion of trapped particles in the Earth's quasi-dipolar magnetic filed and the physical processes occurring in the radiation belts during a geomagnetic storms. It is important to highlight that this guide is not a detailed text book about space physics as it can be found in [Pierrard, 2024] for instance, nor about data processing. It only purpose is to provide the reader with the necessary tools to understand and facilitate their usage of satellite data in the frame of the study of the RBs.

1.1 Radiative space environment of the Earth

1.1.1 Magnetic environment of the Earth

In the Sun's corona, the temperature exceeds 10^6 K so that some particles can escape the Sun attraction. The stream of particles leaving the solar atmosphere is called the solar wind, which is mainly composed by electrons and protons (with about 10% alpha particles). This plasma travels the interplanetary space at supersonic speeds, between 400 km/s near the neutral surface of the heliosphere and 800 km/s near the coronal holes. The solar wind also transports the magnetic field of the sun, forming the interplanetary magnetic field (IMF). The magnetosphere of the Earth results from the interaction of the geomagnetic field and the solar wind. The boundary between the space dominated by the IMF and the space dominated by the magnetic field of the Earth is called the magnetopause. On the day side of the Earth, the magnetosphere is compressed inward to about 10 Earth radii (R_E) due to the pressure of the solar wind. The position of the magnetopause in the day side strongly depends on the condition of the solar wind and

can be pushed back to geostationary distances to the Earth ($\sim 6.6\ R_E$, with $1\ R_E \approx 6371$ km) [Hannu E. J. Koskinen, 2022]. In the night side, the magnetosphere is stretched out up to 100 R_E, creating the magnetotail. It is composed by two lobes of opposite magnetic polarity which are separated by the plasma sheet, composed by hot plasma of both solar and ionospheric origin [Pierrard, 2009]. This constitutes the outer magnetosphere.
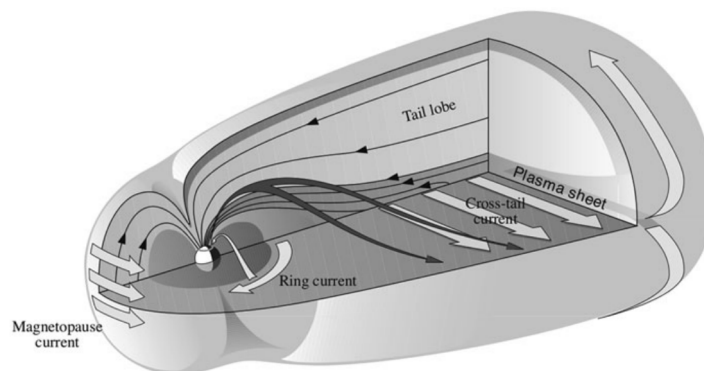
Figure 1.1: Magnetosphere of the Earth. Image from [Hannu E. J. Koskinen, 2022]

The inner magnetosphere is the region where the magnetic field is quasi-dipolar. In this region, one find a variety of particle species with various energy, as well as various spatial distribution:

1. The ring current is generated by the azimuthal drift motion of energetic particles. Electrons move in the eastward direction while positively charged particles move in the westward direction. Particles forming the ring current are located between 3-8 R_E from the Earth [Hannu E. J. Koskinen, 2022].

2. The radiation belts are mainly composed by high energy electrons and protons trapped in the quasi dipolar geomagnetic field. A more detailed explanation of the belts is given in the next section.

3. The plasmasphere is the most inner part of the magnetosphere. It is composed of cold and dense plasma (~ 1 eV) originating from the ionosphere. The limit of the plasmasphere is relatively well defined (rapid drop in the proton density) and is called the plasmapause [Hannu E. J. Koskinen, 2022].

All of those components of the inner magnetosphere spatially overlap and interact with each other. Specifically the plasmapause, whose position strongly depends on the magnetic activity, plays an important role in the dynamics of the outer belt electrons.

1.1.2   The Van Allen radiation belts

The terrestrial radiation belts were discovered in 1958 by James Van Allen and his co-workers with the launch of the first American satellite *Explorer 1*. The spacecraft was equipped with a Geiger-Müller instrument whose goal was to measure cosmic radiation. The instrument worked well up until an altitude of 700 km where the count of the Geiger

instrument suddenly dropped to zero. The satellite was travelling through a region where the radiations were so intense that the instrument was saturated [Pierrard, 2009].

The radiation belts are toroidal regions populated by high energy particles trapped in the magnetic field of the Earth. They mainly consist of electrons and protons (with a very small fraction of heavier ions). The energy range of particles in the radiation belt is comprised between ~ 30 keV to several hundred MeV for protons in the inner belt. There are two distinct radiation belts. The inner belt, located closer to the Earth extends up to 4 R_E in the equatorial plane. It is populated by both electrons and protons of varying energy. The outer belt, which extends from 4 R_E to 10 R_E in the equatorial plane, is composed in majority by electrons. This belt is much more variable in time that the inner one. The two belts are separated by a slot region, where the flux of particles is much lower. The position and the width of the slot, as well as the radiation belts depend on the energy of the electrons [Pierrard, 2009]. It is also interesting to note that a configuration with three belts was observed during one month for ultrarelativistic electrons (E > 3.4 MeV) [Hannu E. J. Koskinen, 2022].

1.1.3 South Atlantic anomaly

The geomagnetic field of the Earth is generated in its liquid core. The axis of the magnetic dipole is not aligned with the rotation axis, an angle of 11° separate them. In addition, the center of the dipole does not coincide with the center of gravity of the Earth. The center of the dipole is 500 km away, toward the northern Pacific. Due to the combination of both offsets (in angle and in position), the intensity of the magnetic field is minimum over the South Atlantic. Moreover, the magnetic dipole axis is the axis of symmetry of the radiation belts. Thus protons of the inner belt are able to penetrate deeper in the atmosphere over this region, which is called the south Atlantic anomaly or SAA. Besides, at a given altitude, the intensity of energetic proton fluxes are much higher over the SAA, which can have impact on LEO orbiting satellites [Pierrard, 2009].
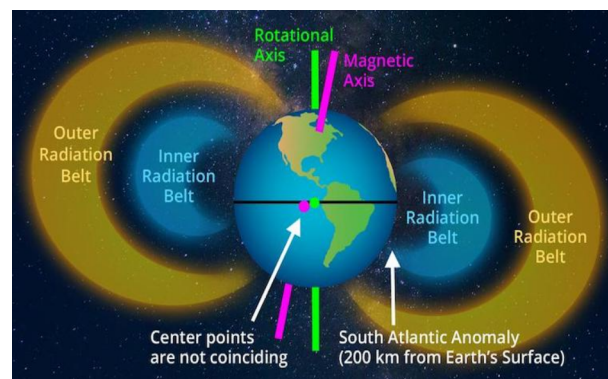

Figure 1.2: Schematic drawing of the Van Allen Radiation belts. The deeper penetration of the inner belt is also represented. This image was taken from https://stellariasacademy.online/south-atlantic-anomaly/20/05/

1.2 Motion of particles in the radiation belts

In the radiation belts, the plasma has a very low density, such that in good approximation, collisions between particles can be neglected and their motion is supposed to be independent from each other. The motion of charged particles is then driven by the Lorentz force acting on them, due to the presence of electric fields as well as geomagnetic field. The equation of motion of a given particle of mass m and charge q in the radiation belts is then given by,

$$m\boldsymbol{a} = q(\boldsymbol{E} + \boldsymbol{v} \wedge \boldsymbol{B}) + m\boldsymbol{g} \tag{1.1}$$

The solution of this equation is very complex but can be obtained numerically. However in order to get a better understanding and insight of the movement of trapped particles, some approximations can be made and their motion can be decomposed in three distinct (quasi-)periodic motions: the gyration motion around a guiding center, the bouncing motion along the magnetic field lines and the azimuthal drift motion [Pierrard, 2009].

1.2.1 Gyration motion

Considering a uniform and static magnetic field $\boldsymbol{B}$ pointing in the $\mathbf{z}$ direction, and neglecting other forces (like gravity and Coulomb force), the equation of motion of a non relativistic charged particles of mass m and charge q is given by,

$$m\frac{d\boldsymbol{p}}{dt} = q\boldsymbol{v} \wedge \boldsymbol{B} \tag{1.2}$$

The motion of the particle described by this equation can be split in two. First the particle orbits a guiding center in the plane perpendicular to the magnetic field. Second, the movement of the guiding center parallel to the magnetic field. [Hannu E. J. Koskinen, 2022] From the circular motion, it is possible to derive the expression of the gyro radius (also called Larmor radius),

$$\rho_G = \frac{mv_\perp}{|q|B} \tag{1.3}$$

where $v_\perp$ is the velocity perpendicular to the magnetic field. The gyro radius depends on the particle species, the energy as well as the intensity of the magnetic field. Thus, for a given particle which guiding center follows a given magnetic field line, its gyro radius is largest at the magnetic equator. The angular frequency of the gyration motion is given by the Larmor angular frequency,

$$\omega_G = \frac{v_\perp}{\rho_G} = \frac{|q|B}{m} \tag{1.4}$$

and the Larmor period is thus,

$$T_G = \frac{2\pi}{\omega_G} = \frac{2\pi m}{|q|B} \tag{1.5}$$

1.2.2 Bouncing motion between mirror points

Let's now consider the magnetic moment associated with the current created by the gyration motion of a particle around its guiding center. It can be defined as the ratio between the kinetic energy transverse to the magnetic field and the intensity of the magnetic field,

$$\mu_B = \frac{1}{2}\frac{mv_\perp^2}{B} \tag{1.6}$$

According to Faraday's law, the magnetic flux through the gyration loop of the particle is constant,

$$\phi = B\pi\rho_G^2 = \frac{2\pi m}{q^2}\mu_B = cst \tag{1.7}$$

Thus, μ_B is also conserved, and since the mass of the particle is constant,

$$\frac{v_\perp^2}{B} = cst \tag{1.8}$$

Due to conservation of the energy, and since $v^2 = v_\perp^2 + v_\parallel^2$, v is also conserved. The pitch angle of the particle is defined as the angle α such that $v_\perp = v\sin\alpha$. By the conservation of the magnetic moment and the definition of the pitch angle,

$$\frac{v^2\sin^2\alpha}{B} = cst \tag{1.9}$$

thus, for a given point at the equator and a point at higher latitude,

$$\frac{\sin^2\alpha_{eq}}{B_{eq}} = \frac{\sin^2\alpha}{B} \tag{1.10}$$

A particle moving from the equator (where the magnetic field is the weakest) to higher latitudes will see increasing intensities of the magnetic field. In order to satisfy the relation above, the pitch angle of the particle must also increase. This will be the case until the pitch angle value reaches 90°. At this point, all the energy of the particle is due to the perpendicular velocity (i.e. $v_\parallel = 0$) and the particle cannot go to higher latitudes, it is called the mirror point. The particle will then move back toward the equator [Pierrard, 2009]. This bounce is caused by the mirror force, created by the gradient of the magnetic field, acting on the magnetic moment of the particle (https://hiddensymmetries.princeton.edu/sites/g/files/toruqf1546/files/single_particle_orbits_sss_final.pdf).

If s is the position of the guiding center along the magnetic filed line and if s_m and s'_m are the coordinates of the mirror points, the bounce period is given by,

$$T_b = 2\int_{s'_m}^{s_m}\frac{ds}{v_\parallel(s)} = \frac{2}{v}\int_{s'_m}^{s_m}\left(1 - \frac{B(s)}{B_m}\right)^{-\frac{1}{2}}ds \tag{1.11}$$

1.2.3   Drift motion

As mentioned in Equation 1.1, particles in the radiation belts are also affected by external forces. If the external forces are perpendicular to the magnetic field (homogeneous and stationary), the particle velocity can be decomposed in a gyration velocity ($\boldsymbol{v}_L$) around the guiding center and the drift velocity of the guiding center ($\boldsymbol{v}_D$), such that $\boldsymbol{v} = \boldsymbol{v}_D + \boldsymbol{v}_L$. From Equation 1.1 it is possible to show that the drift velocity is given by,

$$\boldsymbol{v}_D = \frac{\boldsymbol{F} \wedge \boldsymbol{B}}{qB^2} \tag{1.12}$$

where $\boldsymbol{F}$ are the external forces. The drift velocity is always perpendicular to the magnetic field and the force creating it. The azimuthal drifting motion of particles can lead to the production of electric current which current density is given by,

$$\boldsymbol{J} = ne(v_F^+ - v_F^-) \tag{1.13}$$

assuming quasi-neutrality of the plasma. Here is the list of forces that lead to the drift motion of particles and their contribution to the formation of an electric current,

1. Gravity: $\boldsymbol{F} = m\boldsymbol{g}$. In this case, positively and negatively charged particles drift in opposite directions. Electrons drift to the West, while positive ions drift to the East. The drift velocity is proportional to the mass of the particle and is thus much larger for ions than electrons. This produces an electric current that flows in the opposite directions than the observed ring current.

2. Coulomb force: $\boldsymbol{F} = q\boldsymbol{E}$. In the presence of an electric field, the drift velocity of all species is the same. It does not contribute to the formation of an electric current. In addition to that, if the electric field in the magnetosphere is equal to the co-rotating electric field $\boldsymbol{E}_{corr}$, all particles will drift eastward with the same speed as the Earth's angular speed Ω_E. The co-rotating electric field is given by:

$$\boldsymbol{E}_{corr} = -(\boldsymbol{\Omega} \wedge \boldsymbol{r}) \wedge \boldsymbol{B} \tag{1.14}$$

3. Magnetic field gradient: $\boldsymbol{F} = -\mu_B \boldsymbol{\nabla} B$. This is the force applied by an inhomogeneous magnetic field on the magnetic dipole formed by the gyration motion of the particles. In this case, the drift velocity is proportional to the mass as well as the energy of the particles. In addition to that, the drift of electrons and ions has opposite directions, electrons drift in the eastward direction and positive ions in the westward direction.

$$\boldsymbol{v}_B = \frac{-\mu_B \boldsymbol{\nabla} B \wedge \boldsymbol{B}}{qB^2} \tag{1.15}$$

The guiding center approximation (i.e. the decomposition of the motion in the gyromotion and the motion of the guiding center) holds valid as long as the gyro radius of the particles is much smaller than the characteristic variation distance of the magnetic field, i.e.

$$\rho_G << \frac{B}{|\boldsymbol{\nabla} B|} \tag{1.16}$$

6

The guiding center approximation is also valid if the drift velocity is much smaller than the gyration velocity. For electrons and ions from 1 to 100 keV, the force due to magnetic field inhomogeneity is responsible for the creation of the ring current which in turn is responsible for the weakening of the geomagnetic field during magnetic storms.

4. Curvature of the magnetic field lines. The force in play here is the centrifugal force on the particle caused by the curvature of the field lines and is given by,

$$\boldsymbol{F} = \frac{mv_{\parallel}^2}{R_c}\boldsymbol{n} \tag{1.17}$$

where $R_c = \frac{B}{\nabla B}$ is the curvature radius of the magnetic force lines for rotational-less field and $\boldsymbol{n}$ is the normal unit vector of the field lines and directed outward. The drift speed of trapped particles thus becomes,

$$\boldsymbol{v}_{R_c} = -\frac{mv_{\parallel}^2(\boldsymbol{\nabla}B)_{\perp} \wedge \boldsymbol{B}}{qB^3} \tag{1.18}$$

It is possible to combine the drift motion due to the magnetic force and the curvature of the field line to find and expression for the total drift velocity due the the magnetic field,

$$\boldsymbol{v}_B = \frac{m}{2qB^3}(v_{\parallel}^2 + v_{\perp}^2)\boldsymbol{B} \wedge \boldsymbol{\nabla}B \tag{1.19}$$

Thus, electrons drift to the eastward direction while protons and ions drift in the westward direction.

5. Inertial force. This force appears when the drift velocity of the guiding center is not constant,

$$\boldsymbol{F} = -m\frac{d\boldsymbol{v}_D}{dt} \tag{1.20}$$

Thus if the ambient fields are stationary, i.e $\frac{d\boldsymbol{E}}{dt} = 0$ and $\frac{\boldsymbol{B}}{dt} = 0$ there is no variation in the drift velocity of the guiding center and thus $\boldsymbol{v}_I = 0$. However, if the electric field is not stationary the variation in the drift velocity is only due to the variation of the drift velocity caused by the electric field: $\frac{d\boldsymbol{v}_D}{dt} = \frac{d\boldsymbol{v}_E}{dt}$. Thus the drift velocity due to the inertial force is given by,

$$\boldsymbol{v}_I = -m\frac{\frac{d\boldsymbol{E}}{dt} \wedge \boldsymbol{B}}{qB^2} \wedge \frac{\boldsymbol{B}}{qB^2} = m\frac{\frac{d\boldsymbol{E}}{dt}}{qB^2} \tag{1.21}$$

This drift motion is called the polarisation drift and the resulting electric currents are called polarisation currents.

Particle	ρ_g	$T_g(s)$	$T_b(s)$	$T_D(min)$
Electron (1MeV)	320 m	7×10^{-6}	0.1	50
Proton (10MeV)	30 km	5×10^{-5}	0.65	3.2

Table 1.1: Typical numerical values for the gyration radius ρ_g, gyration period T_g, bounce period T_b and drift period T_D for electrons and protons of the radiation belts [Pierrard, 2009]
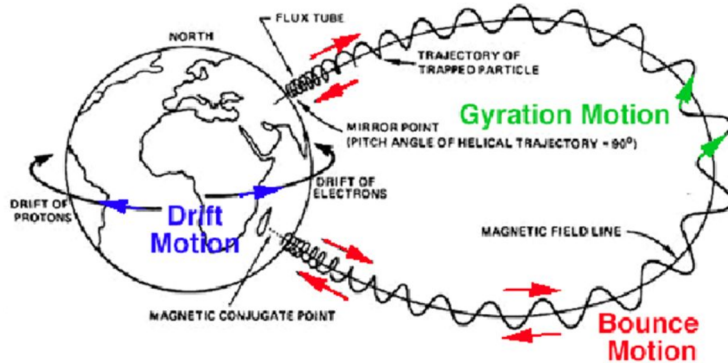
Figure 1.3: Representation of the superimposed motion of trapped particles in the radiation belts.

The total drift velocity of the trapped particles in the geomagnetic field is the sum of all the above mentioned velocities.

$$\boldsymbol{v}_{tot} = \boldsymbol{v}_g + \boldsymbol{v}_E + \boldsymbol{v}_B + \boldsymbol{v}_I \tag{1.22}$$

The importance of those components depends on the energy of the trapped particles as well as the intensity and variability of the electric and magnetic field [Pierrard, 2009].

1.3 Adiabatic invariants

As described above, the motion of trapped particles in the radiation belts can be decomposed in three separate (quasi-)periodic motions. In the context of Hamiltonian mechanics, it is possible to show for quasi-periodic systems that if $\boldsymbol{p}$ is the canonical momentum and $\boldsymbol{q}$ is the canonical coordinates, the following quantity,

$$I = \frac{1}{2\pi} \oint \boldsymbol{p} \cdot d\boldsymbol{q} \tag{1.23}$$

is an adiabatic invariant over the quasi-period [Hannu E. J. Koskinen, 2022] (a proof is given in [Ukhorskiy and Sitnov, 2012]). Such quantities are approximate constants of slowly varying systems (i.e. the variation time scale of the system is much larger than the period of the motion). To each (quasi-)periodic motion found in the belts, it is possible to associate an adiabatic invariant. However, in the belts, rapid variations of the

magnetic field can lead to non-adiabatic motion (i.e. violation of the adiabatic invariants) of particles and significantly contributes to particle losses in the population of the belts.

1.3.1 The first adiabatic invariant

The first adiabatic invariant is associated to the gyro-motion of trapped particles. If the guiding center approximation holds valid, and for $\boldsymbol{\rho}_L$ the canonical coordinate and $\boldsymbol{p}_\perp$ the canonical momentum,

$$I_1 = \frac{1}{2\pi} \oint \boldsymbol{p}_\perp \cdot d\boldsymbol{\rho}_L = \frac{1}{2\pi} \int_0^{2\pi\rho_L} mv_\perp dl = \frac{m}{q}\mu_B \tag{1.24}$$

where $\mu_B = \frac{mv_\perp^2}{2B}$ is the magnetic moment, is an adiabatic invariant. Thus the magnetic moment, and the magnetic flux through the gyration loop ($\phi = \frac{2\pi m}{q^2}\mu_B$) are constants of the motion. As the particle evolves in the magnetic field, its gyration speed will increase as the magnetic field intensity rises in order to satisfy the conservation of μ_B. This acceleration is called the betatron acceleration [Pierrard, 2009].

In practice, this adiabatic invariant is the less susceptible to be violated since the gyro-motion has the smallest period (see Table 1.1) which is almost always smaller than the characteristic time variation of the magnetic field.

1.3.2 The second adiabatic invariant

The second adiabatic invariant is linked to the bouncing motion of the particles between the two mirror points. In this case, the canonical coordinate is reduced to s, the position of the guiding center on the magnetic filed line and the canonical momentum is reduced to the momentum parallel to the magnetic field $p_\parallel$. Thus,

$$I_2 = \frac{1}{2\pi} \oint p_\parallel ds = \frac{1}{2\pi} \oint mv_\parallel ds = cst \tag{1.25}$$

By definition of the pitch angle, $p_\parallel = p\cos\alpha$. For a particle at a mirror point, the pitch angle is equal to 90°, and the magnetic field line is given by B_m. By virtue of Equation 1.10, for all s

$$\frac{\sin^2\alpha(s)}{B(s)} = \frac{1}{B_m} \tag{1.26}$$

Thus, the parallel component of the momentum can be expressed as,

$$p_\parallel(s) = p\sqrt{1 - \sin^2\alpha(s)} = \sqrt{1 - \frac{B(s)}{B_m}} \tag{1.27}$$

Injecting this expression in the integral above results in $I_2 = 2pI$, where

$$I = \int_{s'_m}^{s_m} \left(1 - \frac{B(s)}{B_m}\right)^{\frac{1}{2}} ds \tag{1.28}$$

If the characteristic variation scale of the magnetic field is very large, the magnetic moment and the momentum are conserved and the integral I is constant.

So if the particle move in a region where the intensity of the magnetic field is higher, the mirror points will be located at higher altitudes and thus, the distance travelled between the two mirror points will be smaller. In addition to that, with the conservation of the second adiabatic invariant, the velocity of the guiding center increases. This acceleration is called the Fermi acceleration [Pierrard, 2009].

The violation of the second invariant can occur in region where the variation of the field are fast on distances close to the curvature radius, where the field lines are stretched and when the characteristic time scale of variation of the field are smaller than the bounce period (given by Equation 1.11).

1.3.3 The third adiabatic invariant

The third and last adiabatic invariant is associated with the azimuthal drift motion of the trapped particles. It expresses the conservation of the magnetic flux in the loop formed by a 360° drift motion of the guiding center. It can be expressed as,

$$I_3 = \frac{1}{2\pi} \oint \boldsymbol{A} \cdot d\boldsymbol{l} \tag{1.29}$$

where $\boldsymbol{A}$ is the potential vector of the field and $d\boldsymbol{l}$ is the infinitesimal arc of the drift path of the guiding center [Hannu E. J. Koskinen, 2022]. It can also be written with the form,

$$I_3 = \frac{1}{2\pi} \oint m v_D r d\phi \tag{1.30}$$

where v_D is the drift velocity of the particles, ϕ the azimuthal angle and r the radius of the drift orbit of the particle. Because this last adiabatic invariant is associated to the drift motion which features the largest period, it is the one that is the most frequently violated. This can happen if the variation of the magnetic field is more rapid than the drift period. Wave-particle interactions with ultra low frequency (ULF) oscillations of the magnetic field and small scaled spatial variation of the magnetic field lead to the non conservation of the third invariant. Those processes are involved in the non adiabatic acceleration of electrons in the outer belt [Pierrard, 2009].

1.4 Geomagnetic coordinates (B, L)

Due to the motion of the trapped particles in the geomagnetic field of the Earth, it is often convenient to introduce a new set of coordinates, the geomagnetic (B, L) coordinates. Those coordinates were introduced by McIlwain in 1961 [McIlwain, 1961] in order to solve the problem of mapping observed fluxes of energetic trapped particles. In this coordinate system, B is the intensity of the magnetic field at the point of measure and L is the McIlwain parameter or the magnetic shell parameter.

It gives, for a dipolar magnetic field, the distance at the equator of the magnetic shell of a trapped particle whose pitch angle is 90° at the point of measure [Pierrard, 2009]. The shell parameter is so useful because, by construction, it is constant along the magnetic field lines. Thus each values of L uniquely defines a drift shell on which particles evolve.
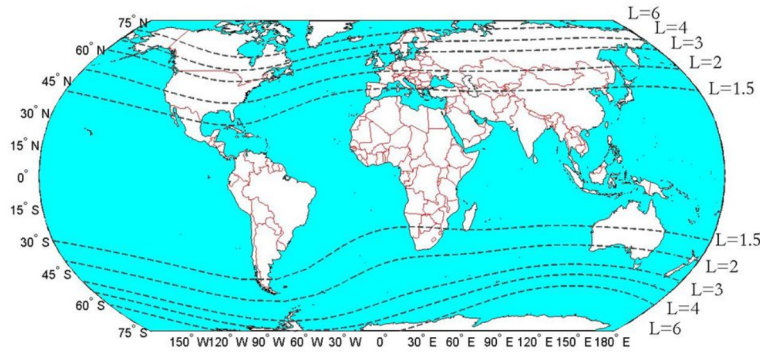
Figure 1.4: Constant L-shell projected on the surface of the Earth.

1.5 Physical processes in the radiation belts

The state of the radiation belts is determined by the balance between the sources of energetic particles and the loss processes affecting them. The difference in temporal, spatial and flux intensity variability between the inner and outer belts indicates that the physical processes occurring in those regions are different. This is due to the fact that the inner and outer belt feature non identical particle populations. In this section, a brief description of the main processes involved in both belts is presented.

1.5.1 Inner belt

The inner belt is mostly populated by high energy protons ranging from several MeV up to GeV. It is very stable in relatively short periods of time and shows variability only during large solar energetic particle (SEP) events that are simultaneous with magnetic storms. However, the inner belt varies in time with the solar cycles. The residence time of protons in the inner belt spreads from several years for proton whose pitch angle is close to the atmospheric loss cones, to several thousands of years for protons mirroring close to the equator [Hannu E. J. Koskinen, 2022].

There are two main sources of high energy protons for the inner belt, cosmic rays and SEP events. When very high energy protons collide with nitrogen or oxygen atoms of the terrestrial atmosphere, neutrons are produced by nuclear reactions. About 10% of the neutrons are traveling away from the Earth and decay into a proton and an electron. Those charged particles are then trapped in the magnetic field of the Earth and form the inner radiation belt. If the source of the incoming proton is cosmic rays, this process is referred as to cosmic ray albedo neutron decay (CRAND). However if the primary proton originates from a strong SEP event, the above mentioned process is called a solar proton albedo neutron decay (SPAND) [Pierrard, 2009]. Protons from SEP events that cannot penetrate in the neutral atmosphere can be directly trapped in the inner belt at $\sim L = 2 - 2.5$ and then radially transported closer to the Earth via radial diffusion.

The loss mechanisms in the inner belts mainly consist of charge exchange and nuclear reactions with neutral atoms present in the exosphere. During a charge exchange, a highly energetic proton collides with a neutral atom and an electron of the neutral atom is transferred to the proton. This leaves a relatively low energy proton that remains

11

trapped in the magnetic field and a very energetic atom that is no more influenced by the electromagnetic fields surrounding the Earth. Nuclear reactions and Coulomb collisions with ionospheric and plasmaspheric ions contribute to the gradual slowing of the protons [Hannu E. J. Koskinen, 2022].

1.5.2   Anisotropic proton fluxes

One of the particularities of the particle fluxes at low altitudes is that the high-energy trapped proton fluxes are strongly anisotropic, i.e., the proton fluxes depend on their arrival direction in the plane perpendicular to the local magnetic field vector as well as on their pitch angle (angle between their velocity vector and the local magnetic field vector). The anisotropy manifests itself through a steep pitch angle distribution and the so-called East-West effect. The pitch angle distribution is due to the particle gyration around magnetic field lines and their mirroring in an inhomogeneous magnetic field. The East-West asymmetry is caused by the finite size of the proton gyroradius and the result of the interaction of the protons with the Earth's magnetosphere. Below 2000 km, the gyroradii of trapped protons with energies > 1 MeV are comparable to the neutral atmospheric scale height. The scale height represents the vertical distance above a planet's surface at which the density or the atmospheric pressure decreases by an exponential factor of e = 2.718. This means that during a gyration, the protons encounter different atmospheric densities, causing differences up to an order of magnitude for fluxes arriving from different azimuths. Due to all those particularities mentioned here above, studying proton fluxes at low altitudes and especially in the South Atlantic Anomaly is very complex. Many parameters need to be taken into account: proton energy, local position, pitch angle, East-West looking direction, solar activity level, solar cycle phase and external sporadic disturbances such as geomagnetic storms or solar energetic particle (SEP) events. When analyzing high energy proton data from instruments at LEO, it is important to take those parameters into account [Pierrard et al., 2023].

1.5.3   Outer belt

The outer belt is populated by high energy electrons and is much more variable in time than the inner belt. The electron fluxes can vary in very short periods of time and so does the spatial extent of the outer belt. The main sources of the outer belt electrons are the solar wind and the ionosphere [Pierrard, 2009]. However, the energies of particles present in the solar wind ($\sim$ keV) and in the Earth ionosphere ($\sim$ eV) are much smaller than the one for radiation belts particles ($\sim$ MeV). There must exist some physical processes that allow the transport of electrons to the radiation belt as well as accelerating them to higher energies. If variations of the magnetic field occur on smaller time scales than the drift motion of the electrons, the violation of the conservation of the third adiabatic invariant causes radial drift motion in the belts. In addition, electrons of the radiation belts interact with plasmaspheric waves that are found in the plasmasphere. The wave-particle interactions have various affects on the electrons populations, such as radial diffusion (interactions with ULF waves) and accelerations (interaction with ULF waves, Whistler-Mode chorus waves) [Hannu E. J. Koskinen, 2022].

Losses of energetic electrons in the outer belt can occur through "real" loss of electrons to the magnetopause or the atmosphere or can be decelerated to very low energy, and thus becoming part of the background plasma. One way that leads to electron losses is the so-called magnetopause shadowing. If electrons of the outer belt are able to cross the magnetopause, they are no longer trapped in Earth's magnetic field and are lost in interplanetary space. The crossing of the outer belt drift shells and the magnetopause has various origins, mainly the drift shell radial expansion during the main phase of magnetic storms and the compression of the magnetopause in the radiation belts [Hannu E. J. Koskinen, 2022]. An other sink for the outer belt electrons is the precipitation in the atmosphere. Interactions between plasmaspheric waves and particles cause pitch angle scattering of the electrons in the atmospheric loss cone, i.e. sufficiently large pitch angle, so that the mirror point of the electrons is located in the atmosphere and they are lost through collisions. Energy scattering of electrons is also possible due to the wave-particle interaction with the various plasma wave found inside and outside the plasmasphere. After being decelerated, the electrons become part of the background low energy plasma [Hannu E. J. Koskinen, 2022].

1.6   Geomagnetic storms

Magnetic or geomagnetic storms are periods during which the magnetic field in the magnetosphere and near the Earth is strongly perturbed. Although it is not unique, the most common planetary index used to detect magnetic storms is the disturbed storm time index (Dst). This index characterizes the intensity of the horizontal component of the magnetic field at the surface of the Earth in equatorial regions. During a storm, the horizontal component of the magnetic field at the surface decreases. This is due to the intensification of the equatorial ring current that tends to reduce the intensity of the geomagnetic field [Pierrard, 2009]. Stormy episodes are distinguished in the Dst time series by inverted peaks. There is no fixed threshold in the Dst that marks a magnetic storms. However, the value of -50 nT is often used as a lower limit for moderate storms. [Koskinen, 2011]. The time extent of geomagnetic storms is between several hours to several days. It corresponds to the time that is necessary to decrease the current density of the ring current by reducing the energy of ions and electrons that it contains but also by lowering its density through precipitation into the atmosphere [Pierrard, 2009].
A geomagnetic storm unfolds in 3 phases,

1. The initial phase differs between storms. The length of the initial phase depends on the structure of the solar wind that drives the storm. If the IMF is directed southward, the initial phase is very short and the main phase of the storm is almost immediate. Some storms also begin with sudden commencements (SC), i.e a sudden increase in the Dst index before the main phase (see Figure 1.5). This commencement is due to the solar wind shock wave hitting the magnetopause [Koskinen, 2011].

2. The main phase is the period during which the horizontal component of the magnetic field and thus the Dst index reaches a minimum value. It is caused by the increase in density of the ring current as well as the acceleration of the particles forming it by the solar wind.
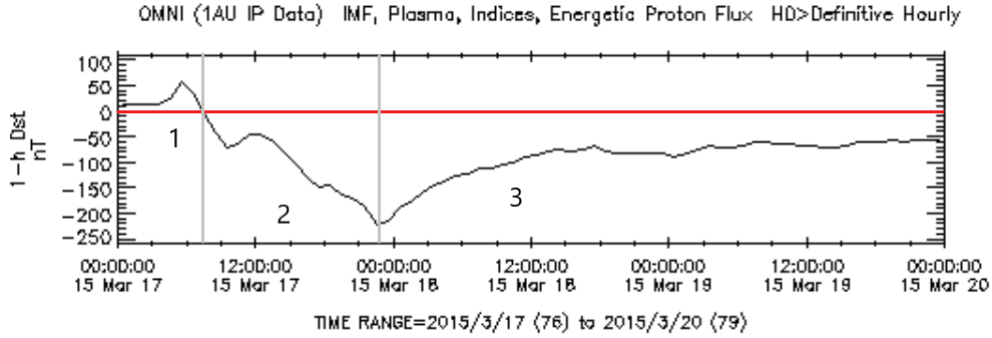
Figure 1.5: Evolution of the Dst index during the storm of March 17, 2015. The red line shows the constant zero value of the Dst. The different numbers correspond to the phases of the magnetic storm. 1. The initial phase with a sudden commencement (SC). 2. The main phase of the storm. 3. The recovery phase. This image has been generated on the NASA website: https://cdaweb.gsfc.nasa.gov/index.html

3. The recovery phase starts when the input of energy and particles of the solar wind comes to an end. The time spread of the recovery phase is much larger than for the main phase, it can last several days. The reason for such a gap in the main and recovery phase time scales is that the physical process leading to the loss of energetic particles in the ring current are much slower than during the injections.

The formation of magnetic storms at least requires that the IMF has a strong southward component for a relatively long period of time (∼3 h) [Koskinen, 2011]. Several phenomena can fulfill those conditions, such as fast solar wind or more extreme events like Solar Energetic Particle events (SEP). SEP events are characterized by the large flux increase of electrons, protons and heavier ions to energies much higher than average. In some very extreme events, protons energies can reach GeV [Klein and Dalla, 2017].

Chapter 2

Flux Analysis

2.1 Open data sources

In space physics, satellite data are often provided in open access to any interested scientists. When using such data, it is important to contact the Principal Investigator (PI) of the instrument to be sure to properly analyze validated and appropriate data. The team who has developed the instrument can give more detailed information on the contamination or data quality. This can complete the data information generally provided at the source that allows to take into account the levels of data (how they have been transformed) and provide the quality flag indicating the relevance of each measurement.

2.2 Differential flux and integral flux

The crucial quantity that is need for the study of the radiation belts is the flux of trapped and/or precipitating particles. This flux is measured in situ by spectrometers or particle telescopes aboard satellites, each with distinct orbits that explore various regions of the radiation belts. Despite differences in measurement techniques and satellite orbits, these instruments primarily yield a similar data product: the particle flux (J). This encompasses electrons and protons, providing observations at specific points in space.

It is essential to differentiate between the *differential flux* and the *integral flux* which are both omnipresent in the in the data products. Onboard spectrometers and particle telescopes measure particle flux within specific energy channels, with the flux in a given channel referred to as the *differential flux* and expressed in $(cm^2 \ s \ sr \ MeV)^{-1}$. Typically, data products are presented as differential flux, along with the energy range of the channel in which they are measured.

However, there are instances where only the *integral flux* is provided. In such cases, it represents the flux of all particles measured above a specified energy threshold, often applicable to protons for characterizing Solar Energetic Particle events. The integral flux is expressed in $(cm^2 \ s)^{-1}$.

The integral flux is easily retrieved given the differential flux. Strictly speaking, we integrate the differential flux with respect to the energy and on all solid angles. In practice, we proceed to the following sum,

$$J_{int}(E > E_0) = 4\pi \sum_{i=0}^{N} J_{diff}(E_i) \; \Delta E_i \qquad (2.1)$$

where $J_{diff}(E_i)$ is the differential flux measured in the energy bin i and ΔE_i is the width of the channel i. Thus, the integral flux does not depend on the energy anymore, although it depends on the lowest energy threshold (E_0).

2.3 Displaying data

In most cases, data products include more than just the differential or integral fluxes. Alongside the time of measurements, the spacecraft's position, intensity of magnetic field components, McIlwain parameter values, and other pertinent parameters for radiation belt studies are commonly provided. It's important to note that these parameters can vary between data products, often due to differences in satellite orbits or aim of the missions.

The most straightforward method to represent particle fluxes is by plotting the flux time series for the relevant channel (if using the differential flux). While this approach is the simplest for visualizing the evolution of particle fluxes in the radiation belts, it may offer limited insights into RBs dynamics. This method could be used to identify events characterized by significant increases or decreases.
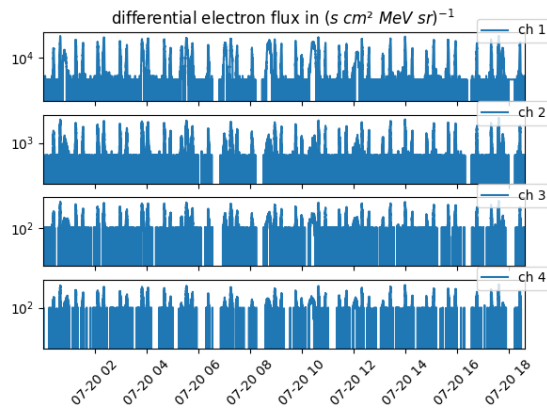

Figure 2.1: Electron differential flux measured by the Energetic Particle Telescope (EPT) in 4 energy channels. ch1: 0.5-0.6 MeV, ch2: 0.6-0.7 MeV, ch3: 0.7-0.8 MeV and ch4: 0.8, 1.0 MeV.

The reason why plotting flux time series isn't the most convenient way to visualize this data is due to the fact that to location of measurement also varies in time. Indeed the satellites along their orbit pass through different regions of the RB, which feature different flux intensities. For example, the electron RBs feature a *slot region*, where the flux sharply decreases across the whole energy spectrum between the outer and the inner belt. As the orbit of the satellite will cross this depleted region, the electron flux in the time series will suddenly drop. Thus, flux variations in the most simple time series the dynamics of the RBs is often more difficult to analyse.

16

A clever work around for this issue is to plot flux time series at "fixed" locations of the RBs. In order to do so, the McIlwain parameter L, which is constructed from a quasi-invariant of the motion of trapped particles, can be used.
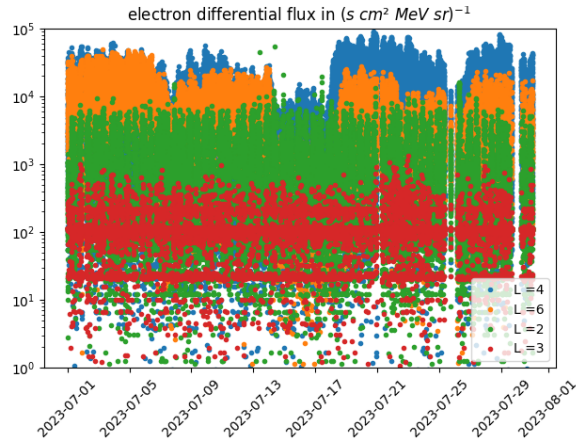

Figure 2.2: Electron differential flux measured by the Energetic Particle Telescope (EPT) in the first energy channel (0.5-0.6 MeV) at different values of L

The most common way to represent RBs particle fluxes is to plot the flux as both a function of time and L as shown in Fig.2.3. This way of displaying has the advantage of showing the evolution in time of the flux along each magnetic shells (labeled by L) on which trapped particles move. With this method, the entire structure of the RBs can be easily observed. In the figure, both the inner and outer belts can be clearly observed at $L = [1, 2.5]$ and $L = [3.5, 8]$ respectively. In the range $L = [2.5, 3.5]$ the region depleted of electron, called the slot, can be observed. From this figure, the dynamics of the radiation belts can be studied.

This figure illustrates well the issue that was mentioned earlier with plotting the data as simple flux time series. Indeed, it appears clearly now that as the instrument's position varies in space, the magnetic shell on which the flux of particles is measured also changes. Hence if the satellite crosses the slot region through its orbit, the flux sharply decreases in a small amount of time. Differentiating true variation of the flux or an effect of the satellite orbit is not an easy task to do if the McIlwain parameter (or another invariant quantity of the trapped particles motion) is used to identify which region of the belts is probed.

As it was mentioned above, parameters provided in the data products can differ from one another. Some parameters offer various ways to explore the data and study the RBs, all of which cannot be shown in this guide. However, if the satellite carrying the instrument is on a Low Earht Orbit (LEO), the longitude and latitude of the satellite are often provided along with the data. This allows to create maps of the radiation belt and study their spatial distribution as shown in Fig.2.4. In this case, for electrons, the three major regions of the RBs are also visible. The narrow bands of intense fluxes at high latitude in both hemispheres are the electron fluxes of the outer belt. The outer belt can be observed in both hemispheres due to the topology of the magnetic field and the oscillation motion of trapped particles along the magnetic filed lines. The inner radiation belt can be observed on the map above the south Atlantic, where the electron fluxes are
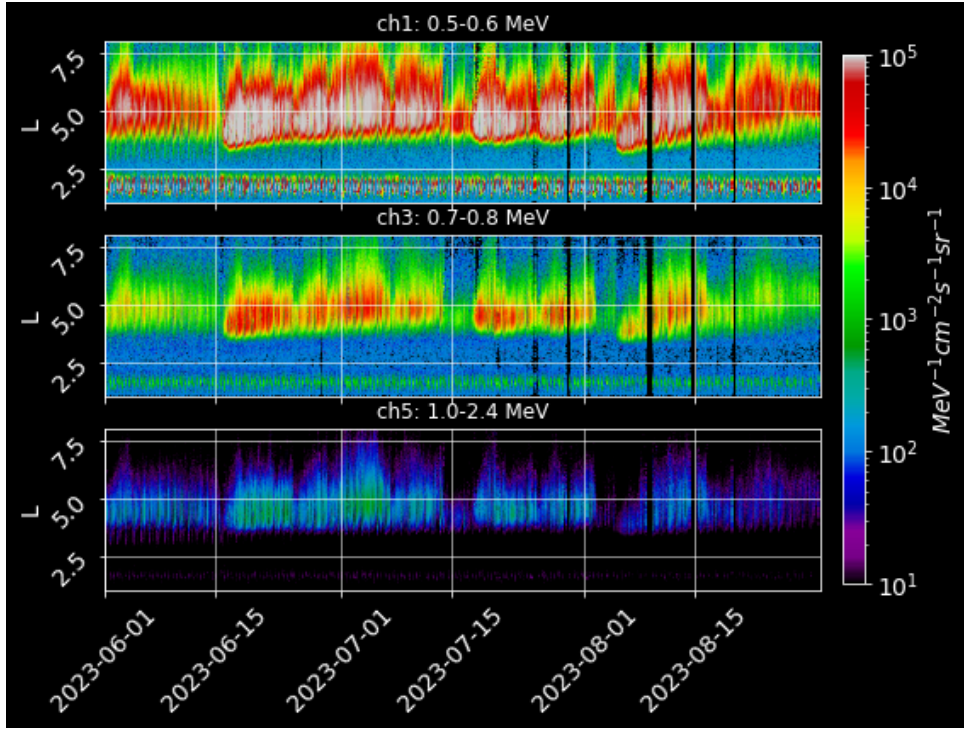
Figure 2.3: Electron differential flux as a function of *L* and time, as measured in the first three channels of the EPT during the first measurement campaign of the EURAMET BIOSPHERE project, from June 1st 2023 to August 31st 2023. The channel energy width are the following, ch1: 0.5-0.6 MeV, ch3: 0.7-0.8 MeV, ch5: 1.0-2.4 MeV

also high. At the altitude at which the EPT is in orbit, at ~ 820 km, the inner belt can only be observed over the south Atlantic due to the South Atlantic Anomaly, a region where the intensity of the Earth geomagnetic filed is lower than anywhere else. Due to the weaker magnetic intensity, trapped particles are able to penetrate at lower altitudes. Of course, the inner belt also exist at other longitudes but at higher altitudes. The slot region in the map correspond to the all the latitudes between the southern and northern edges of the outer belt.

Representing the data in the fashion is convenient because it is to interpret, however it is important to keep in mind that a large amount of data is needed to produce this kind of figure. Indeed, in Fig.2.4, three months of observations from the EPT have been used. Because LEO satellites have a short orbit period and geomagnetic storms occur over the course of a few hours, visualizing the changes in the RBs dynamics on a maps is not convenient. The method is particularly suited to study the long term variations of the belts.

2.4 Data contamination and data quality

Instruments dedicated to accurately measure RBs fluxes can differentiate between particle types and resolve their energy spectra. However, the harsh RBs environment implies potential data contamination. Contamination may arise from other types of energetic particles in the vicinity, particularly in the inner radiation belt where electrons and pro-
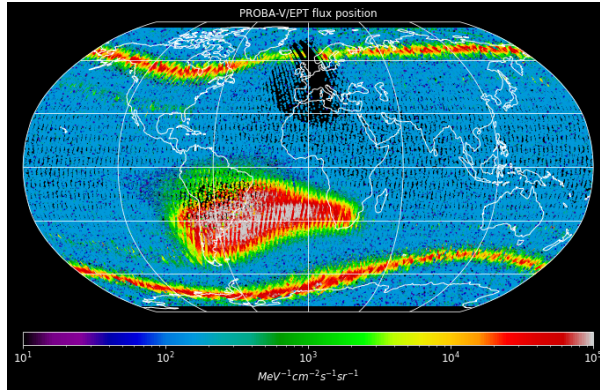
Figure 2.4: Map of the electron differential fluxes measured by the EPT in the first energy channel (0.5-0.6 MeV) during the first measurement campaign of the EURAMET BIOSPHERE project, from June 1st 2023 to August 31st 2023.

tons coexist. In such cases, some protons may be misinterpreted as high-energy electrons, introducing inaccuracies in the data Another source of contamination occurs when particles outside the instruments' field of view strike the detector
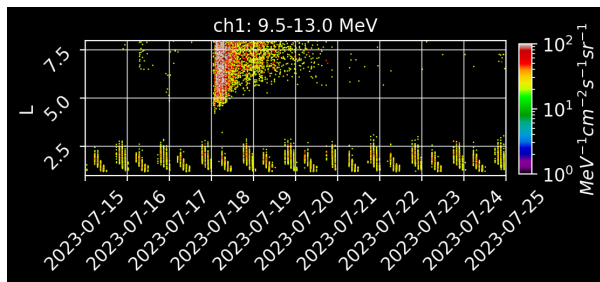

Figure 2.5: Differential proton flux measured by the EPT in the first energy channel during a SEP event in July 2023

As an example of data contamination with data from the EPT, Fig.2.6 shows fluxes of electrons measured during a Solar Energetic Particle (SEP) event that took place in July 2023. The top panel shows the unfiltered data and the bottom panel the filtered data according to the quality flags of the data product. The injection of solar protons in the outer radiation belt begins at high L values and penetrates the belt towards lower L see Fig.2.5. Those protons of high energy are sometimes recorded by the instrument as lower energy electrons, causing the seemingly high electron fluxes at high L. However, the data quality flags provided in the EPT data product label those measurements as contaminated and must be removed from the data the is used for investigation purposes.

Due to those potential sources of contamination, data products often include indicators of data quality, such as quality flags, to convey the confidence level in the data. Understanding how these flags should be used is crucial, as misuse can significantly impact investigation results. Quality flags are typically provided by the instrument development team, and their interpretation may vary between data products. It is highly recommended to contact the Principal Investigator (PI) of the instruments to ensure accurate use and prevent errors when working with the data.
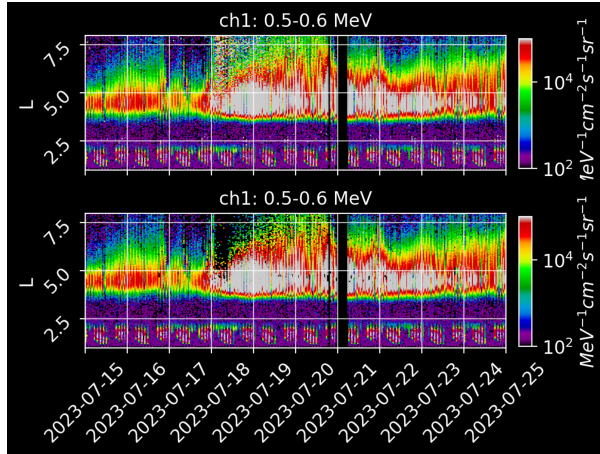
Figure 2.6: Top: Unfiltered electron differential flux observed by the EPT during a SEP event in July 2023. Contamination by proton present in the outer belt. Bottom: Filtered electron differential flux observed by the EPT during a SEP event in July 2023. Contamination by energetic protons has been removed

2.5 Averaging the data in time

Onboard spectrometers and particles telescopes can measure particle fluxes with a very high resolution, for example, the EPT records the flux every 2s. This is of course very useful, but it also leads to a very large amount of data, and in some cases, such a high resolution is not needed (normalizing data for a prediction model, comparing observations from different instruments, ...). Then it makes sense to average the data over longer periods of time. However, performing time averages is not as straightforward as to take all the data and averaging the flux over the desired time interval. The reason for this is again the time dependent position of the observation location. The problem here is that if one was to simply take the time average of all the measurements and parameters provided in the data product, all the positions at which the instrument measured the flux during the given time span would also be averaged. And since the structure of the RBs is such that some regions feature higher fluxes than others, averaging the location of the instrument would lead to large errors in the averaged fluxes, and in any position dependent parameters. Of course, the error will be proportional to the time span on which the average is performed. If the data is averaged every minute, errors on the position of the instrument and thus on the flux will likely be negligible, however, if the time window for the average is one hour or even a day simple averaging of the data is pointless. It is important to keep in mind that this source of error is also highly dependent on the orbit of the instrument carrier.

Considering that this issue is caused by time dependent position of the observation site, satellites which frequently traverse the different regions of the RBs are more susceptible this source of error through time average. For instance, the Geostationary Operational Environmental Satellite (GOES) is on a geostationary orbit, at $L \sim 6.6$, always performs it's measurements in the outer radiation belts, on magnetic shells that are close to one another. At contrary, PROBA-V/EPT is on an heliosynchronous LEO orbit at an altitude of ~ 820 km, with this orbit, the satellite revolves around the Earth in approximately
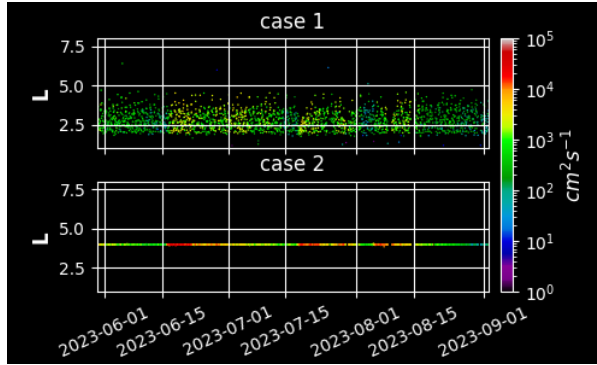
Figure 2.7: This figure shows the flux as a function of time and L, the McIlwain parameter for two different ways to average the data. Case 1 (top) Averaging EPT data on time before setting a L shell. Case 2 (bottom) Setting $L = 4 \pm 0.25$ before averaging on time

110 minutes rapidly crossing all magnetic shells and thus measuring fluxes in all three different RBs regions.

The workaround to this difficulty is to set the location of of the observations and then average in time the data that was observed at this location. In most cases, the parameter to use to set an observation location in the RBs is the McIlwain parameter or an equivalent parameter. Fixing a value of L will ensure that all measurements of particle fluxes occur on the same magnetic shell. However, depending on the averaging time span and the amount of available date, larger/smaller *aera* around the targeted L value must be defined in order to ensure that the averaged flux is statistically relevant.

As an example of how just averaging the data can affect the flux and the other parameters Fig.2.7 uses data from the EPT measured during the first measurement campaign of the EURAMET BIOSPHERE project, plotted as a function of time and L. This figure shows the *'wrong/naive'* and the *'good'* approach to average the data.

In this example, the data is averaged over one hour. The top panel of Fig.2.7 shows the hourly-averaged electron flux in the first energy channel (0.5-0.6 MeV) as a function of time and L. Note that this panel actually is a simple hour average of Fig.2.3. Now, the structure of the RBs has completely vanished, all measurements are located between $L = 2$ and $L = 5$. Also the averaged flux intensity is significantly lower than it is observed with the high resolution. What happens here, in the case of the EPT, is that the a averaging period is that was chosen is about half of the orbit period of the instrument. So the top panel of Fig.2.7 shows the average flux measured and average L value of the EPT over half of its orbit, which is not representative at all of the actual hourly-averaged flux in the radiation belts. In the bottom panel of the figure, only data observed between $L = 3.75$ and $L = 4.25$ were averaged.

Fig.2.8 shows EPT data from the first measurement campaign hourly averaged in L bins of a width of $0.2L$. It appears clearly that by first setting a bin of L in which the data is the averaged on time allows to preserve the structure and the flux intensities that were observed in the high resolution data. Here the example has been presented with the McIlwain parameter, however, the same issue will arise with any position dependent parameter (e.g. the longitude and latitude in the case of averaging the flux on a map). The same method should then be applied to those parameters.
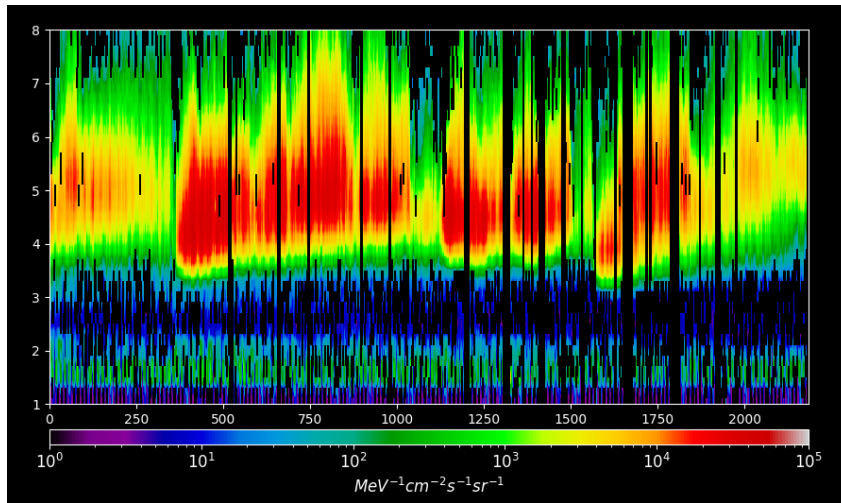
21

Figure 2.8: Hourly-averaged electrons differential flux of the EPT in the first energy channel between June 1st 2023 to August 31st 2023.

Bibliography

[Hannu E. J. Koskinen, 2022] Hannu E. J. Koskinen, E. K. J. K. (2022). *Physics of Earth's Radiation Belts*. Springer.

[Klein and Dalla, 2017] Klein, K.-L. and Dalla, S. (2017). Acceleration and propagation of solar energetic particles. *Space Science Reviews*, 212(3):1107–1136.

[Koskinen, 2011] Koskinen, H. E. (2011). Magnetospheric storms and substorms. In *Physics of Space Storms*, pages 323–370. Springer.

[McIlwain, 1961] McIlwain, C. E. (1961). Coordinates for mapping the distribution of magnetically trapped particles. *Journal of Geophysical Research*, 66(11):3681–3691.

[Pierrard, 2009] Pierrard, V. (2009). *L'Environnement Spatial de la Terre*. Presses universitaires de Louvain.

[Pierrard, 2024] Pierrard, V. (2024). *Effects of the Sun on the space environment of the Earth*. Presses universitaires de Louvain.

[Pierrard et al., 2023] Pierrard, V., Benck, S., Botek, E., Borisov, S., and Winant, A. (2023). Proton flux variations during solar energetic particle events, minimum and maximum solar activity, and splitting of the proton belt in the south atlantic anomaly. *Journal of Geophysical Research: Space Physics*.

[Ukhorskiy and Sitnov, 2012] Ukhorskiy, A. and Sitnov, M. (2012). Dynamics of radiation belt particles. *The van allen probes mission*, pages 545–578.